THE BELL SYSTEM
TECHNICAL JOURNAL

DEVOTED TO THE SCIENTIFIC AND ENGINEERING
ASPECTS OF ELECTRICAL COMMUNICATION

Volume 56 May 1977 Number 5

Impact of Microwave Depolarization During Multipath Fading on Digital Radio Performance

By S. H. LIN

(Manuscript received October 20, 1976)

Experimental data describing the statistics of microwave depolarization during multipath fading have been obtained from a propagation experiment conducted near Atlanta, Georgia. The experiment included 6- and 11-GHz reception on a 26.4-mile path, and 11-GHz reception on a 15.9-mile path. A theoretical model, suggested by T. O. Mottl, indicates that the interference occasioned by depolarization for a given copolarized signal level is Rice-Nakagami distributed. The theoretically calculated distribution agrees well with the data. The cross-polarization interference consists of a signal-level-dependent component as well as a residual that is independent of the in-line signal level. The residual is Rayleigh distributed with an rms value about 40 dB below the nonfaded in-line signal level, and limits the multipath fade margin of a cochannel dual-polarized digital radio to approximately 30 dB. Calculated multipath outage probabilities for cochannel, dual-polarized, 11-GHz, quaternary-coherent-phase-shift-keyed digital radios with and without space-diversity protection are presented.

I. INTRODUCTION

Maintaining adequate cross-polarization discrimination (XPD) is important to both analog and digital radio transmission systems. For analog radio and single polarization digital radio, adequate XPD allows reduction of frequency separation between cross-polarized, adjacent channels to increase the transmission capacity. This is known as inter-

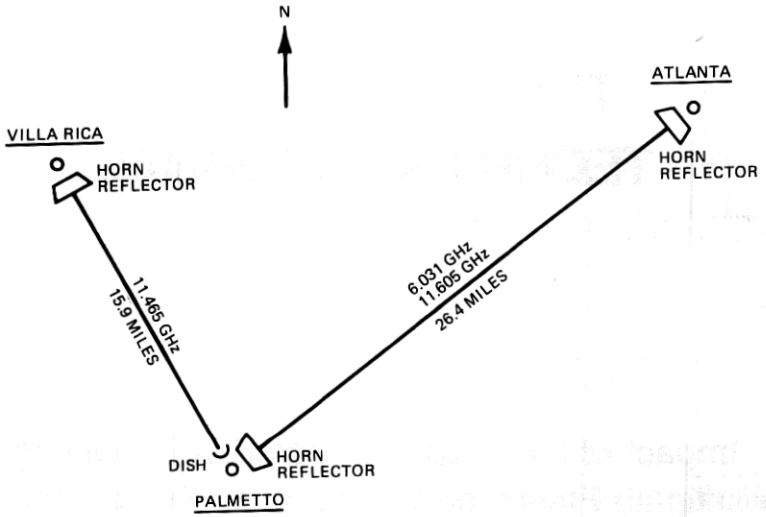

Fig. 1—Path layout, frequencies, and antennas for microwave propagation experiments near Atlanta, Georgia.

stitial operation in channel allocation of analog radio. Some digital radio may also rely on XPD to achieve high transmission capacity by a two-channel-per-frequency allocation in which both orthogonal linear polarizations in the same frequency band are employed as two independent transmission paths.

References 1 to 5 indicate that XPD can degrade significantly during multipath fading. Therefore, statistics of XPD during multipath fading are needed to assess the performance and reliability of both analog and digital radio. Section II of this paper describes a propagation experiment, the measured data, and a theoretical model for microwave depolarization during multipath fading. Section III applies these results to calculate the multipath-caused outages of dual-polarization 11-GHz quaternary-coherent-phase-shift-keyed (QCPSK) digital radio. A companion paper[6] by T. O. Mottl gives greater details on outage probabilities of QCPSK digital radio.

II. MICROWAVE DEPOLARIZATION DURING MULTIPATH FADING

2.1 Introduction

Section 2.2 describes microwave propagation experiments; Section 2.3 presents multipath fading and associated depolarization statistics including cumulative amplitude distributions, number of fades, and average fade durations. Section 2.4 discusses a theoretical model, suggested by T. O. Mottl,[6] to describe the behavior of XPD during multipath fading.

Table I — Path parameters of microwave propagation experiments near Atlanta, Georgia

Path	Path Length Miles	Km	Freq. (GHz)	(v_{xp}) rms when $V_{IL} = 0$ dB (dB)	K (dB)	ϵ_{rms} (dB)	Transmitter Polarization	r
Atlanta-Palmetto	26.4	42.5	6.031	−25.9	−25.9	−47.6	Vertical	0.13
Atlanta-Palmetto	26.4	42.5	11.605	−19.5	−19.6	−36.3	Vertical	0.4
Villa Rica-Palmetto	15.9	25.6	11.465	−42.7	−46.2	−45.3	Vertical	0.015

r = Multipath fade occurrence factor defined in eqs. (32) and (33).
$v_{xp} = |kv_{IL} + \epsilon e^{j\phi}|$

2.2 *Microwave propagation experiments*

Figure 1 displays the path layout for the Palmetto propagation experiment. Two vertically polarized signals with frequencies of 6.031 and 11.605 GHz are transmitted over the 26.4-mile path from Atlanta to Palmetto, and one vertically polarized signal with a frequency of 11.465 GHz is transmitted over the 15.9-mile path from Villa Rica to Palmetto. At Palmetto, the common receiving site, the levels of both vertically and horizontally polarized received signals are recorded.

Both the transmitter and the receiver on the Atlanta-Palmetto path employ standard Bell System horn reflector antennas, waveguides, and channel separation networks.[7,8] Circular waveguide (WC281) simultaneously supports both polarizations of the 6- and 11-GHz signals. On the Villa Rica-Palmetto path, a standard Bell System horn reflector antenna, waveguide, and network are used to transmit the 11-GHz signal. The 11-GHz receiver at Palmetto utilizes a 6-foot dish antenna with two elliptical waveguides to separately carry two orthogonally polarized received signals.

The measured cross-polarization discrimination (XPD) obtaining on these paths during nonfading periods is listed in Table I. The best performance is 42.7 dB on the 11-GHz Villa Rica-Palmetto path; the worst, 19.5 dB on the 11-GHz Atlanta path. Poor XPD on the 11-GHz Atlanta-Palmetto path is believed due to the 4- and 6-GHz channel-separation networks at both transmitting and receiving ends, as well as the fact that this link requires quite long waveguides (see Table II).* The WC281 waveguide is an overmoded guide at the 11-GHz frequency, which supports 21 higher-order modes in addition to the desired fundamental.[9] Slight imperfections on this long (see Table I) waveguide run can cause mode coupling with resultant depolarization.[10] The imper-

* The high fill of radio traffic on this link limits opportunity to study the hardware impact on 11-GHz XPD.

Table II — Waveguide types and lengths

Station	Waveguide Length (ft)	Waveguide Type
	A. Atlanta-Palmetto Path	
Atlanta	75	EW-107
	15	WR-90
	20	WC-281
Palmetto	54	EW-107
	5	WR-90 Flex-guide
	300	WC-281
	B. Villa Rica-Palmetto Path	
Villa Rica	85	Elliptical
	21	WR-90
	170	WC-281
Palmetto	80	Elliptical

fections in antennas, antenna misalignment, and channel-separation networks also contribute to depolarization.

In the following, the in-line signal refers to the received (vertically polarized) signal which is "in-line" with the transmitted signal; the cross-polarization interference refers to the received horizontally polarized signal which is orthogonal to it.

2.3 Experimental Data

The experimental data obtained during the 6.5-month period from August 15, 1974 to February 28, 1975 have been processed.

2.3.1 Statistics of in-line signals

The measured statistics of multipath fading of the in-line signals are shown in Figs. 2, 3, and 4 for the cumulative amplitude distribution, the number of fades, and the average fade durations, respectively, as functions of fade depth.

In the deep-fade region ($\geqq$20 dB), the slopes of the distributions in Figs. 2, 3, and 4 are consistent with the theoretical distribution for deep fades.[11–14] The cumulative amplitude distribution has an inverse slope of 10 dB per decade of probability, the number of fades has an inverse slope of 20 dB per decade of number of fades, and the average fade duration has an inverse slope of 20 dB per decade of duration.

2.3.2 Statistics of cross-polarization interference

Let $v_{IL}(t)$ and $v_{xp}(t)$ be the time varying amplitudes of the in-line signal voltage and the depolarized (interference) voltage, respectively, both normalized to the nonfaded in-line signal voltage. The cross-polarization discrimination (XPD) can be written as

$$\text{XPD} = 20 \log_{10}(v_{IL}/v_{xp}), \text{ dB} \quad (1)$$

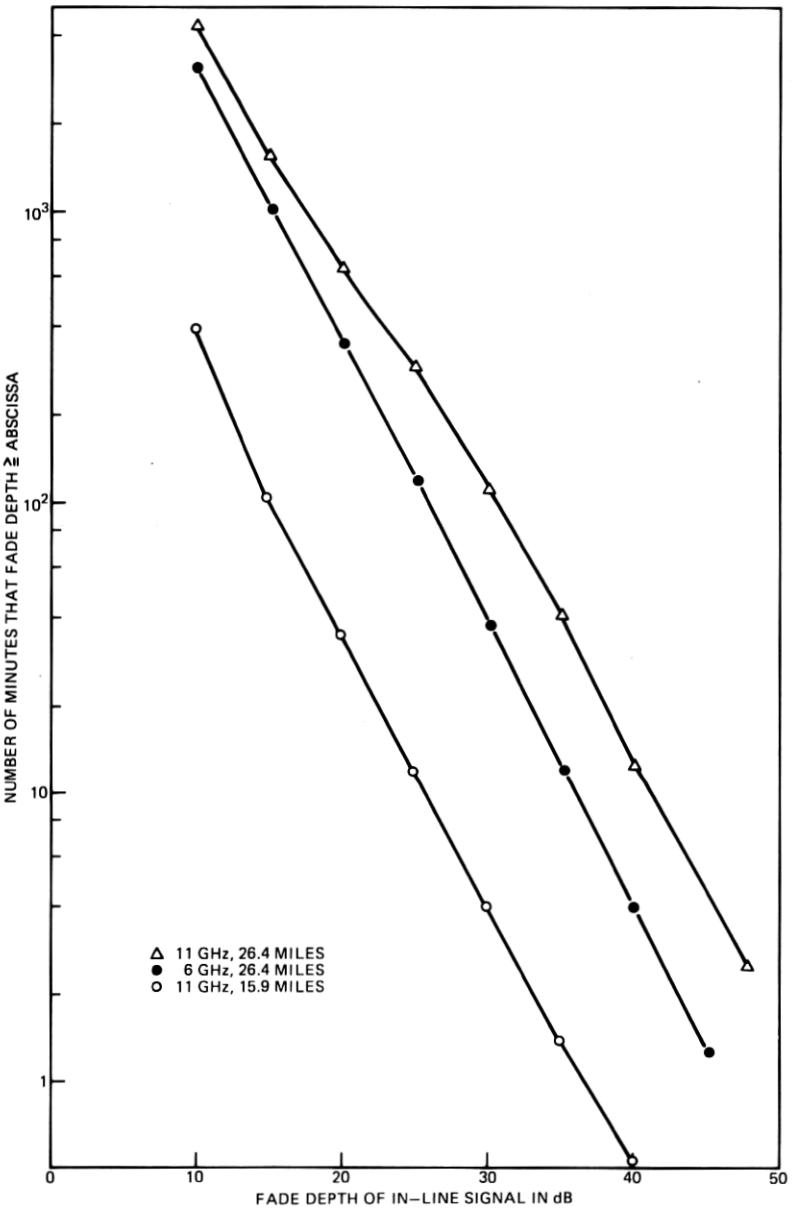

Fig. 2—Measured 6.5-month data (August 15, 1974 to February 28, 1975) on the cumulative amplitude distributions of in-line signals during multipath fading.

$$= V_{\mathrm{IL}} - V_{xp}, \tag{2}$$

where

$$V_{\mathrm{IL}} \equiv 20 \log_{10} v_{\mathrm{IL}} \text{ dB} \tag{3}$$

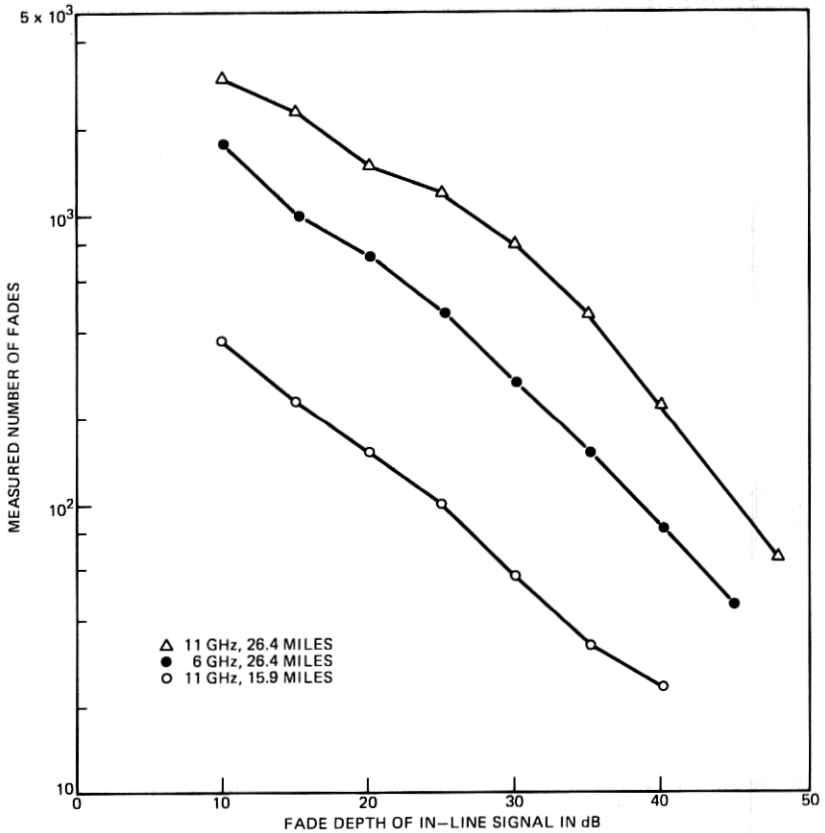

Fig. 3—Measured 6.5-month data (August 15, 1974 to February 28, 1975) on number of fades of in-line signals during multipath fading.

is the time-varying, in-line signal level in dB with respect to its nonfaded level, and

$$V_{xp} \equiv 20 \log_{10} v_{xp} \text{ dB} \tag{4}$$

is the time-varying, depolarized component of the signal measured (in dB) with respect to the nonfaded level of in-line signal.

Figure 5 shows fluctuations of V_{IL} and V_{xp} measured on the 11-GHz, Atlanta-Palmetto path during a typical nonfading hour. Both V_{IL} and V_{xp} scintillate but approximately 20 dB of XPD is maintained. Figure 6 shows the behavior of V_{IL} and V_{xp} during a multipath fading hour. In the 40-minute period from 8:00 a.m. to 8:40 a.m., the variations of V_{IL} and V_{xp} appear to be relatively well correlated. However, at 8:44 a.m., V_{IL} suffers a 35-dB fade, whereas V_{xp} undergoes only a 15-dB fade (from −20 dB to −35 dB), thereby degrading the XPD to 0 dB. In other words, at this moment, the signal received at the cross-polarized feed (inter-

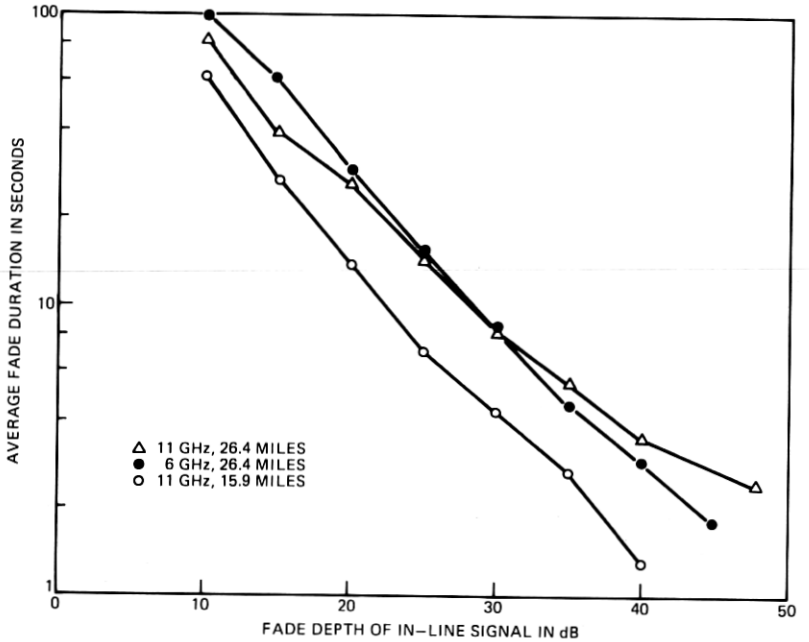

Fig. 4—Measured 6.5-month data (August 15, 1974 to February 28, 1975) on average fade durations of in-line signals during multipath fading.

ference to a signal normally transmitted with horizontal polarization that has faded with the same amount as V_{IL}) is as strong as the desired horizontally polarized in-line signal and will prevent useful transmission of data over the channel; hence, an outage is caused to a 2-channel-per-frequency-assignment digital radio. Figure 7 shows another example of depolarizing fading on the 11-GHz, Villa Rica-Palmetto path.

Although rain also causes depolarization, the measured XPD is generally better than 10 dB, even during rain fades in excess of 40 dB. Depolarization during multipath is therefore considerably more serious than rain-caused depolarization in Western U.S.A., where rain-caused outage is not the dominant controlling factor on radio-system reliability.

Figures 8 through 10 display the rms value of v_{xp} conditioned to the fade depth of the in-line signal v_{IL}. In the shallow fade region (i.e., $V_{IL} \geqq -10$ dB), $(V_{xp})_{rms}$ decreases almost linearly (dB by dB) with V_{IL}; whereas in the deep-fade region (i.e., $V_{IL} < -20$ dB), $(V_{xp})_{rms}$ approaches a residual level, becoming independent of V_{IL} as V_{IL} decreases. The residual depolarized component in these three sets are between 37 and 50 dB below the nonfaded in-line signal level.

Figures 11 through 13 show the probability distributions of V_{xp}, conditioned to a given fade depth of in-line signal, plotted on Rayleigh

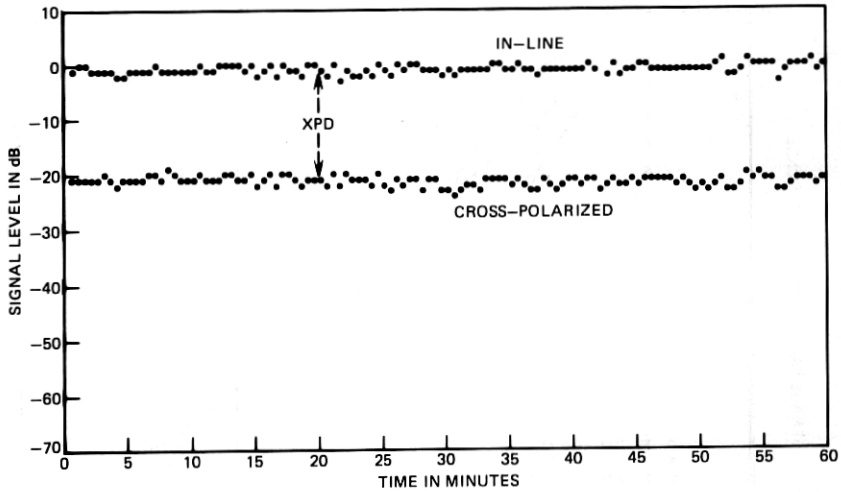

Fig. 5—Scintillations of in-line signal and cross-polarization interference on the 11-GHz 26.4-mile path (Atlanta-Palmetto) during a nonfading hour—August 28, 1974; 12:00 A.M. to 1:00 P.M.

probability paper. For deep fades of in-line signal (i.e., $V_{IL} \leqq -30$ dB), the probability distributions of V_{xp} are approximately Rayleigh. This Rayleigh distribution of V_{xp}, conditioned to deep fades of in-line signal, was reported earlier in Ref. 1.

The solid lines in Figs. 8 through 13 are calculated results from a theoretical model discussed in the next section.

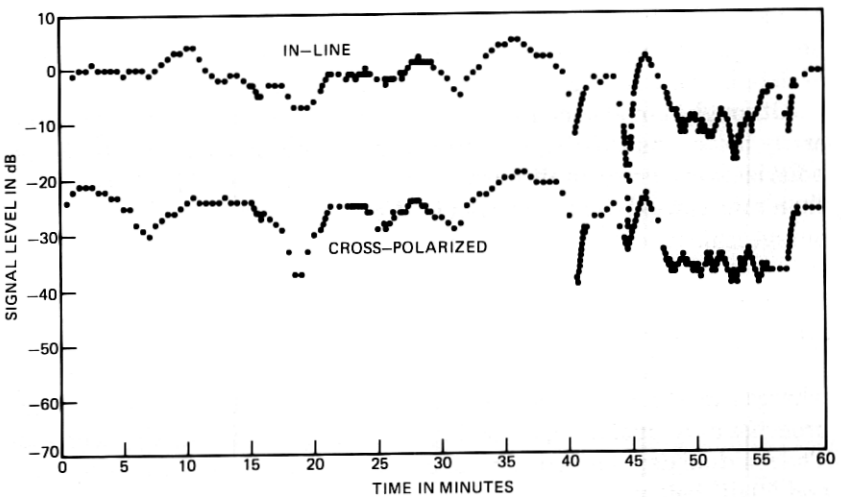

Fig. 6—Fading behavior of in-line signal and cross-polarization interference on the 11-GHz 26.4-mile path (Atlanta-Palmetto) during a multipath fading hour—August 23, 1974; 8:00 A.M. to 9:00 A.M.

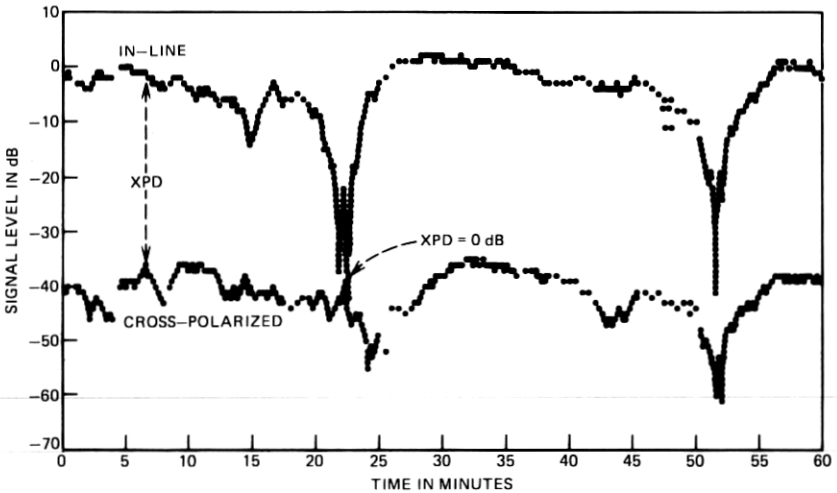

Fig. 7—Fading behavior of in-line signal and cross-polarization interference on the 11-GHz 15.9-mile path (Villa Rica-Palmetto) during a multipath fading hour—November 2, 1974; 9:00 A.M. to 10:00 A.M.

2.4 Theoretical model

Based on early observations similar to those displayed in Figs. 6 through 10, Mottl[6] suggests decomposition of the cross-polarization interference v_{xp} into two components:

$$v_{xp} \equiv |kv_{\mathrm{IL}} + \epsilon e^{j\phi}|, \tag{5}$$

where k is a proportionality constant, and ϕ is the relative phase between the proportionate component and the residual component.

For shallow fades of the in-line signal, v_{xp} is dominated by kv_{IL}, and decreases linearly with v_{IL}. During deep fades of the in-line signal, v_{xp} is dominated by ϵ, which is independent of v_{IL}. During deep fades of in-line signal, the probability distribution of v_{xp} is essentially that of ϵ. The data in Figs. 11 through 13 indicate the conditional distribution of v_{xp}. It is seen that ϵ is approximately Rayleigh, a single parameter distribution uniquely determined by its rms value. The rms values, ϵ_{rms}, are obtained from the measured distribution of v_{xp} during deep fades of v_{IL} and they range from −36 to −48 dB, as listed in Table I.

For a given in-line signal level, eq. (5) indicates that v_{xp} consists of a constant vector [i.e., kv_{IL}] plus a Rayleigh vector. Such interpretation immediately implies that, for a given in-line signal level, the cross-polarization interference, v_{xp}, is Rice-Nakagami distributed.[15–17] In other words, the conditional distribution of v_{xp} can be written as

$$P(v_{xp} \geqq a|v_{\mathrm{IL}}) = \int_a^\infty p(v_{xp}|v_{\mathrm{IL}})dv_{xp}, \tag{6}$$

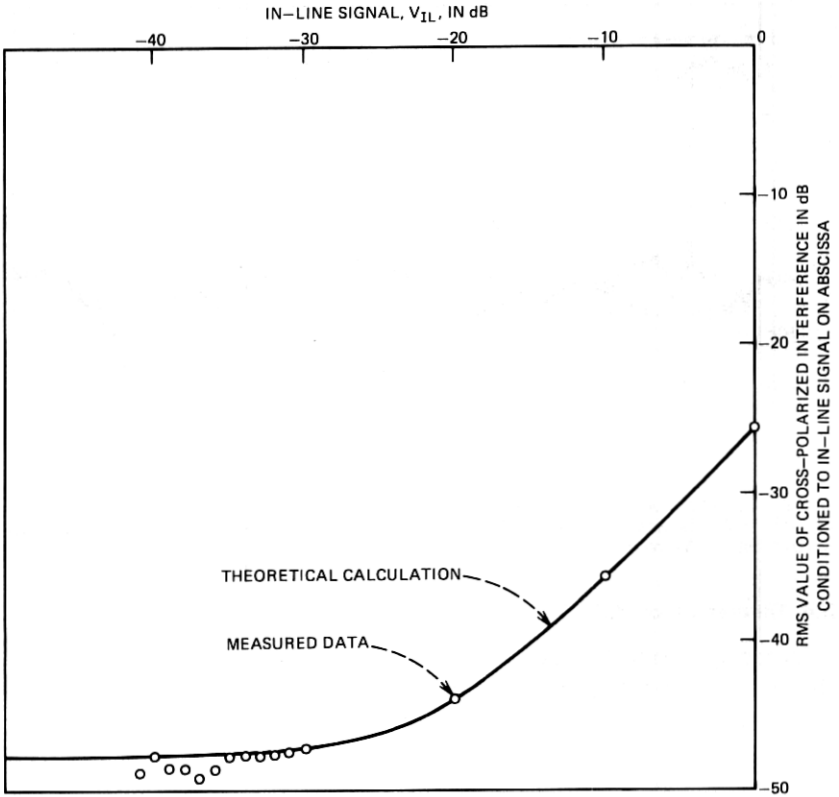

Fig. 8—Dependence of rms value of cross-polarization interference on in-line signal level measured on the 6-GHz 26.4-mile path (Atlanta-Palmetto); measured 6.5-month data (August 15, 1974 to February 28, 1975).

where

$$p(v_{xp}|v_{IL}) = \left[\frac{2v_{xp}}{\epsilon^2_{rms}} \exp - \left(\frac{v^2_{xp} + k^2 v^2_{IL}}{\epsilon^2_{rms}}\right)\right]\left[I_0\left(\frac{2v_{xp}kv_{IL}}{\epsilon^2_{rms}}\right)\right] \quad (7)$$

and $I_0(\sim)$ denotes the modified Bessel function of zeroth order. Based on the well-known properties of this Rice-Nakagami distribution,[15–17] it is easily shown that

$$[v_{xp}(v_{IL})]_{rms} = [k^2 v^2_{IL} + \epsilon^2_{rms}]^{1/2} \quad (8)$$

from which,

$$k = \frac{1}{v_{IL}}\{[v_{xp}(v_{IL})]^2_{rms} - \epsilon^2_{rms}\}^{1/2} \quad (9)$$

for any v_{IL}, where $v_{xp}(v_{IL})$ denotes v_{xp} conditioned to a given v_{IL}. This equation shows that the proportionality constant k in eq. (5) can be

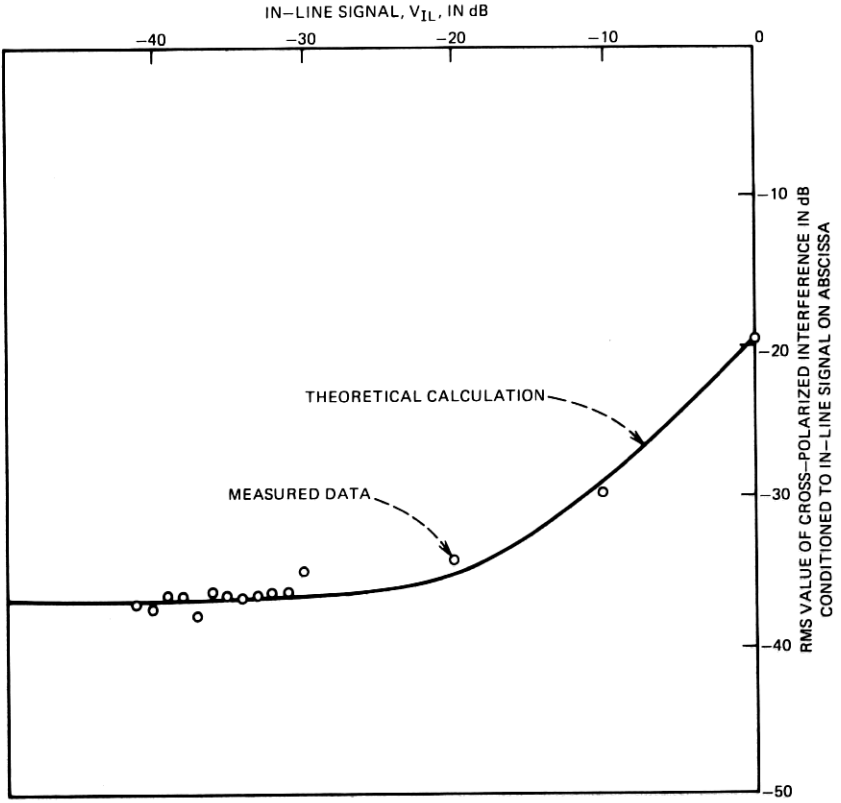

Fig. 9—Dependence of rms value of cross-polarization interference on in-line signal measured on the 11-GHz 26.4-mile path (Atlanta-Palmetto); measured 6.5-month data (August 15, 1974 to February 28, 1975).

calculated from measured values of $[v_{xp}(v_{IL})]_{rms}$ and ϵ_{rms}. For example, the data in Fig. 9 for the 11-GHz Atlanta-Palmetto path indicate

$$[v_{xp}(v_{IL} = 0 \text{ dB})]_{rms} = -19.5 \text{ dB} \tag{10}$$

and

$$\epsilon_{rms} = [v_{xp}(v_{IL} \leqq 30 \text{ dB})]_{rms} = -36.3 \text{ dB}. \tag{11}$$

Substituting (10) and (11) into (9) yields

$$k = 0.105 \tag{12}$$

from which

$$K = 20 \log_{10} k = -19.6 \text{ dB}. \tag{13}$$

Table I lists estimated values of K for all three sets of data.

The Rice-Nakagami distribution (7) for v_{xp} is completely determined

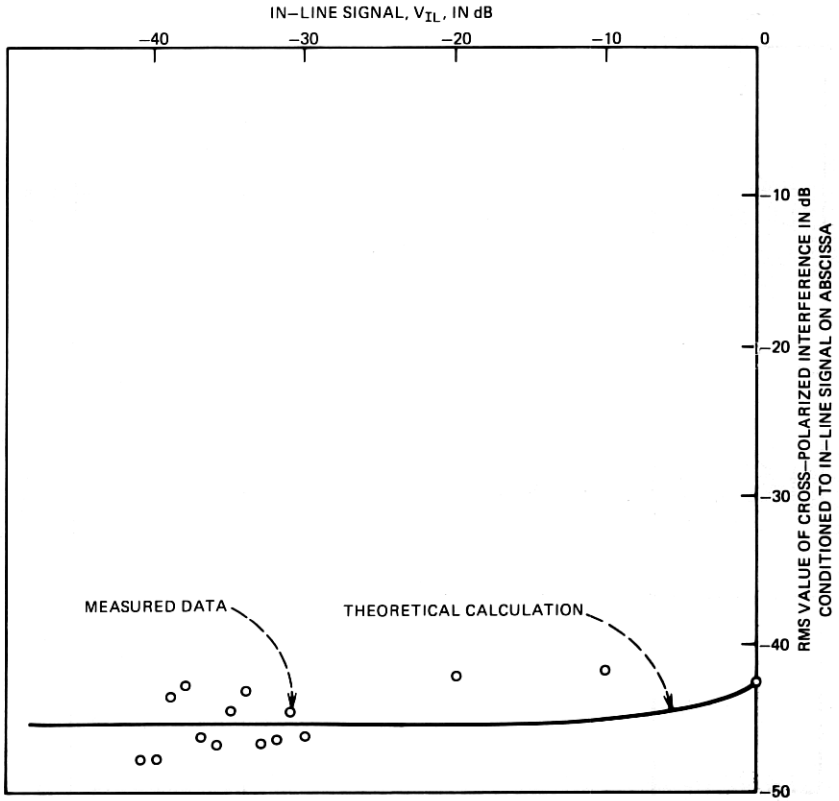

Fig. 10—Dependence of rms value of cross-polarization interference on in-line signal level measured on the 11-GHz 15.9-mile path (Villa Rica-Palmetto); measured 6.5-month data (August 15, 1974 to February 28, 1975).

by two parameters: ϵ_{rms} and k. Since these two parameters are obtained from the measured data, the Rice-Nakagami distribution of v_{xp} for any v_{IL} can be calculated. Figures 11 through 13 show that the theoretical distributions (solid lines) calculated from the two parameters (ϵ_{rms} and k) agree very well with the measured data.

Similarly, eq. (8) indicates that $[v_{xp}(v_{\text{IL}})]_{\text{rms}}$ for any v_{IL} is also completely determined by the same parameters: ϵ_{rms} and k. Figures 8 through 10 show that the theoretical dependence of $[v_{xp}(v_{\text{IL}})]_{\text{rms}}$ calculated by eq. (8) also agrees closely with the data.

At the present time, the physical interpretation of the theoretical model (5) is speculative. The proportionality constant k may be related to antenna alignment, imperfections in the antennas, the waveguides, or the channel-separation networks (designed for transmission of the fundamental mode). In other words, the proportional component, kv_{IL}, may be controllable by reducing these imperfections. On the other hand,

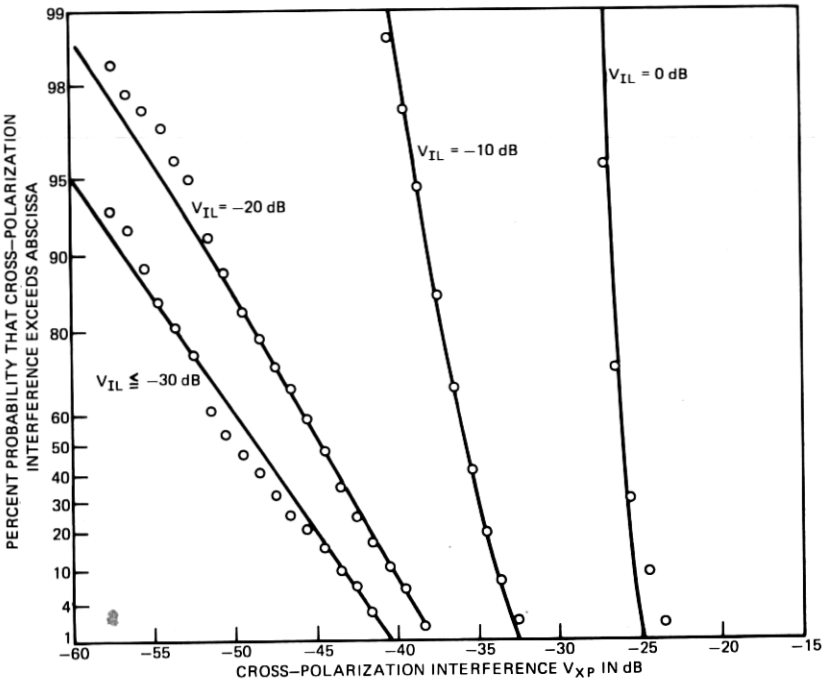

Fig. 11—Rice-Nakagami distribution (with Rayleigh probability coordinates) of cross-polarization interference, V_{xp}, conditioned to a given in-line signal level, V_{IL}, and measured on the 6-GHz 26.4-mile path (Atlanta-Palmetto). The circles are measured 6.5-month data (August 15, 1974 to February 28, 1975).

the Rayleigh distribution of the residual cross-polarized component, ϵ, suggests that ϵ may represent the sum of many small depolarized components due to, say, foreground scattering,* the antenna cross-polarization response to off-axis incoming rays, or the excitation of higher-order modes in the waveguides by the off-axis incoming rays.†

For successful isolation of the two information channels of a dual-polarized digital radio system, it is reasonable to expect that

$$K = 20 \log_{10} k \leqq -20 \text{ dB}. \tag{14}$$

Since the correlated component, kv_{IL}, of cross-polarization interference always fades simultaneously with the desired signal and maintains a carrier-to-interference ratio (CIR) of 20 dB or better, the degradation of radio fade margin due to the correlated components, kv_{IL}, is quite

* In the multipath propagation condition, the relative amplitudes and phases of the foreground scattered components are quite different from those of direct paths. Therefore, the sum of foreground scattered components is decorrelated from the sum of the direct paths.

† Waveguide imperfections may couple depolarized components through higher-order modes. Since these are dispersed[18,19] in the circular waveguide and antenna responses to off-axis incoming rays are mode-dependent, their sum is decorrelated from v_{IL}.

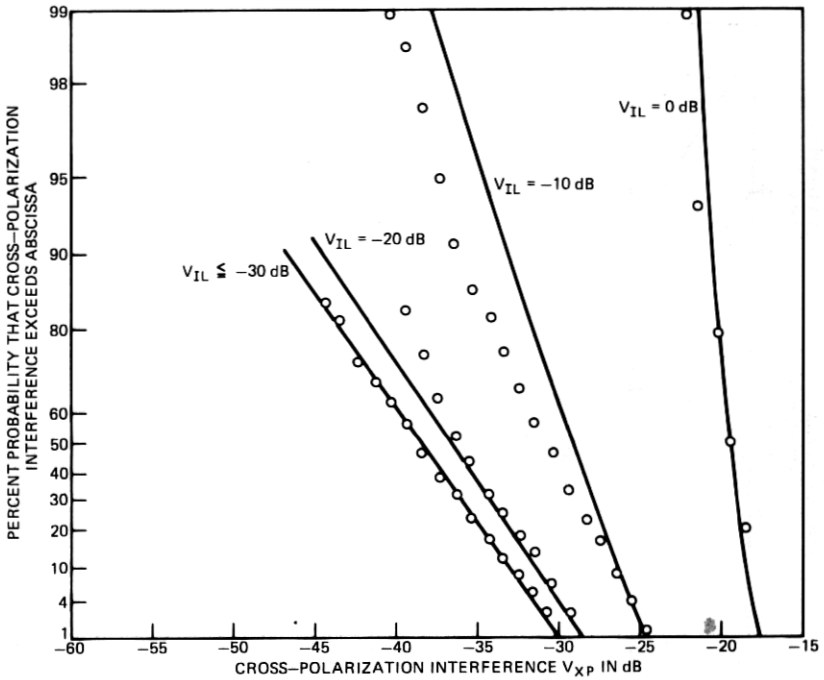

Fig. 12—Rice-Nakagami distribution (with Rayleigh probability coordinates) of cross-polarization interference, V_{xp}, conditioned to a given in-line signal level, V_{IL}, and measured on the 11-GHz 26.4-mile path (Atlanta-Palmetto). The circles are measured 6.5-month data (August 15, 1974 to February 28, 1975).

small, say 2 dB or less. On the other hand, the residual cross-polarization interference ϵ, being independent of the desired signal, will limit fade margin. For example, for a typical 11-GHz digital radio, the thermal noise is about 60 dB below the nonfaded signal, whereas ϵ_{rms} is only about 40 dB below the nonfaded signal (see Table I). Therefore, the residual cross-polarization interference may reduce the fade margin by as much as 20 dB and greatly increase the "multipath caused" outages.

III. MULTIPATH OUTAGES OF DUAL-POLARIZATION, 11-GHz, PHASE-SHIFT-KEYED DIGITAL RADIO

3.1 Introduction

Section 3.2 presents a model for the performance of quaternary-coherent-phase-shift-keyed (QCPSK) digital radio subjected to interference and noise. Section 3.3 outlines the procedure and states the assumptions needed for calculation of multipath-caused outage probabilities of dual-polarization, 11-GHz, QCPSK digital radio. Section 3.4 summarizes the results of outage calculations.

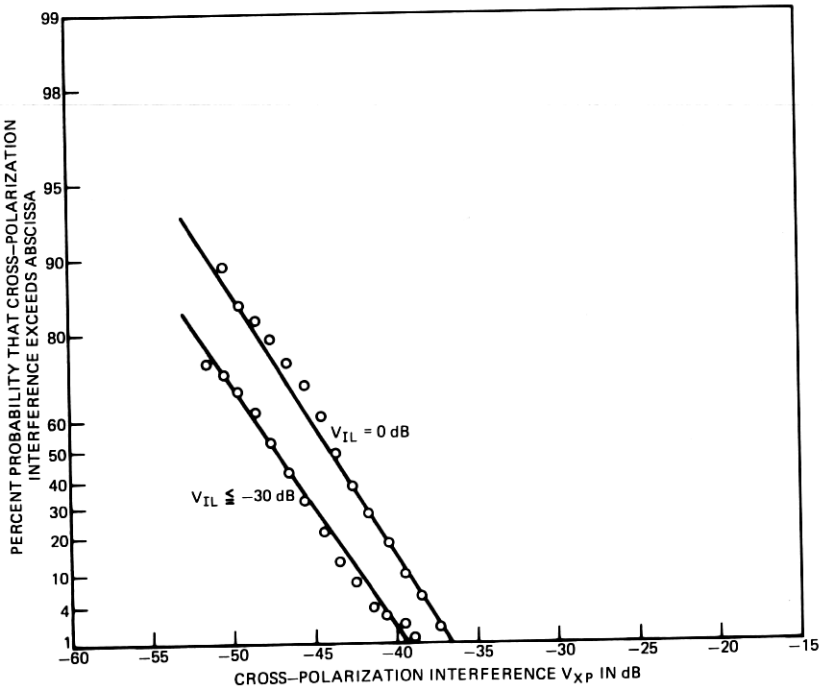

Fig. 13—Rice-Nakagami distribution (with Rayleigh probability coordinates) of cross-polarization interference, V_{xp}, conditioned to a given in-line signal level, V_{IL}, measured on the 11-GHz 15.9-mile path (Villa Rica-Palmetto). The circles are measured 6.5-month data (August 15, 1974 to February 28, 1975).

Rain-caused outage probabilities of 11-GHz radio is treated elsewhere.[20,21] This paper, therefore, treats only multipath-caused outages.

3.2 Digital radio model

We model the cochannel, dual-polarization, 11-GHz digital radio as a QCPSK system corrupted by complex gaussian noise with one major interference representing the depolarized component of the cochannel cross-polarized signal.

Both noise and interference cause digital transmission errors. Figure 14 shows the relationship between the carrier-to-noise ratio (CNR) and carrier-to-interference ratio (CIR) for a fixed bit-error-rate (BER). In Fig. 14 the circles represent the measured performance[22] of a prototype QCPSK digital radio; the solid lines are approximations described by

$$10^{-\frac{\mathrm{CNR}}{10}} + 10^{-\frac{\mathrm{CIR}+\Delta}{10}} = 10^{-\frac{\mathrm{CNR}_a}{10}}, \qquad (15)$$

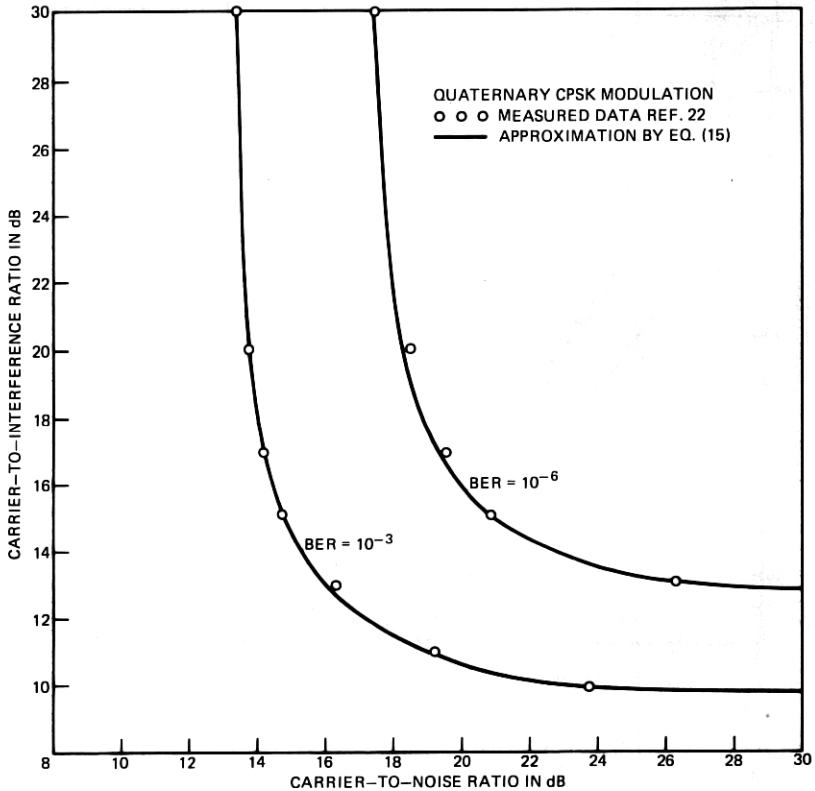

Fig. 14—Relationship between carrier-to-interference ratio and carrier-to- noise ratio for a given bit-error-rate (BER) of QCPSK radio.

or equivalently,

$$\text{CIR} = -10 \log_{10} \left\{ 10^{-\frac{\text{CNR}_a}{10}} - 10^{-\frac{\text{CNR}}{10}} \right\} - \Delta, \tag{16}$$

where

$$\text{CNR}_a = \begin{cases} 13.4 \text{ dB for BER} = 10^{-3} & (17) \\ 17.4 \text{ dB for BER} = 10^{-6} & (18) \end{cases}$$

and

$$\Delta = \begin{cases} 3.8 \text{ dB for BER} = 10^{-3} & (19) \\ 4.8 \text{ dB for BER} = 10^{-6} & (20) \end{cases}$$

Equation (15) means that for a given BER threshold, the interference power reduced by Δ dB plus noise power is a constant. In other words,

the QCPSK radio system is more resistant to interference than to noise by Δ dB.

The probability of outage of the QCPSK radio for a given BER threshold is simply the integral of the joint CNR, CIR probability density function over the two-dimensional region lying below the BER threshold curve in Fig. 14. This double integration is carried out by eqs. (27) and (31) in the next section.

3.3 Outline of the outage estimation procedure

(a) The nonfaded carrier-to-noise ratio, CNR_{NF}, for a reference 25-mile hop length is assumed to be 67.4 dB.[22]

(b) The dependence of CNR_{NF} on hop length D is

$$\text{CNR}_{\text{NF}}(D) = \text{CNR}_{\text{NF}}(D_0) - 20 \log \frac{D}{D_0}, \tag{21}$$

where

$$D_0 = 25 \text{ miles}. \tag{22}$$

(c) With the desired, in-line signal faded α dB, the effective $\text{CNR}(D)$ for path length D is:

$$\text{CNR}(D) = \text{CNR}_{\text{NF}}(D) - \alpha, \tag{23}$$

where

$$\alpha = -20 \log_{10} v_{\text{IL}}, \text{ dB}. \tag{24}$$

(d) For a given BER (say 10^{-3}) at outage threshold, the CNR versus CIR curve in Fig. 14 means that the cross-polarization interference, v_{xpo}, at outage threshold is a function of in-line signal level, v_{IL}. By combining eqs. (15), (23), and (24), it can be shown that

$$v_{xpo}(v_{\text{IL}}) = v_{\text{IL}} \left\{ 10^{-\frac{\text{CNR}_a}{10}} - 10^{-\frac{\text{CNR}_{\text{NF}} - \alpha}{10}} \right\}^{1/2} 10^{\frac{\Delta}{20}}. \tag{25}$$

(e) For a given in-line signal level, the probability of outage is

$$P(\text{outage} | v_{\text{IL}}) = P(v_{xp} \geqq v_{xpo} | v_{\text{IL}}) \tag{26}$$

$$= \int_{v_{xpo}}^{\infty} p(v_{xp} | v_{\text{IL}}) dv_{xp}, \tag{27}$$

where $p(v_{xp} | v_{\text{IL}})$ is given by eq. (7).

(f) The distribution of the in-line signal, v_{IL}, without diversity protection is assumed to be Rayleigh, i.e.,

$$p(v_{\text{IL}}) = 2 v_{\text{IL}} e^{-v_{\text{IL}}^2}. \tag{28}$$

(g) The distribution of the in-line signal, v_{IL}, with space diversity and selective switching is[23,24]

$$p(v_{IL}) = \frac{8v_{IL}}{(1-\rho^2)} \int_0^{v_{IL}} z \left[I_0 \left(\frac{2\rho z v_{IL}}{1-\rho^2} \right) \right] \exp - \left(\frac{z^2 + v_{IL}^2}{1-\rho^2} \right) dz, \tag{29}$$

where ρ^2 is approximately equal to the correlation coefficient between the two input signals received from the space-diversity antenna pair.[25] The dependence of ρ^2 on antenna spacing S is obtained empirically as[26,27]

$$\rho^2 = 1 - 7 \times 10^{-5} \frac{S^2 f}{D}, \tag{30}$$

where

S = antenna center-to-center separation in feet,
f = radio frequency in GHz,
D = path length in miles.

Strictly speaking, assumptions (f) and (g) are valid only for the deep-fade region, but not the shallow-fade region. However, outages occur mostly in the deep-fade region (see Figs. 15 and 16), therefore, assumptions (f) and (g) are acceptable for outage calculations.

Notice that the selective-switching scheme always connects the receiver to the better one of the two input signals and is an idealized switch. In practice, there are many different ways of utilizing the two input-diversity signals. For example, threshold-blind switching provides less improvement, whereas equal-gain combining or maximum-ratio combining provides more improvement than the selective switching.[12] Furthermore, a digital radio may be caused to switch at a given error-rate threshold rather than through the signal amplitudes of the two input signals. In this paper, we use selective switching for ease of computation and thus provide only an estimation of feasible diversity improvement. A full-scale investigation of various diversity-protection schemes is beyond the scope of this paper.

(h) The total outage probability is

$$\begin{aligned} P_{\text{outage}} &= \int_0^\infty P(\text{outage}|v_{IL})[p(v_{IL})dv_{IL}] \\ &= \int_0^\infty P(v_{xp} \geqq v_{xpo}|v_{IL})[p(v_{IL})dv_{IL}] \end{aligned} \tag{31}$$

and the total two-way outage time is

$$T_{\text{outage}} = 2rT_0P_{\text{outage}} \text{ minutes/year}, \tag{32}$$

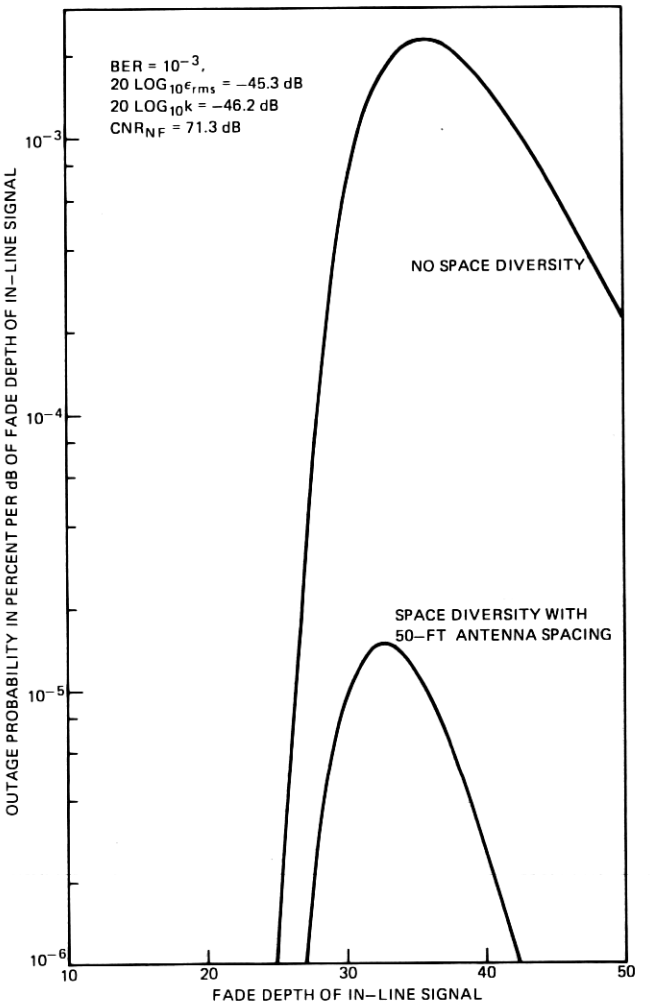

Fig. 15—Dependence of one-way outage probability density function on multipath fade depth of in-line signal of 11-GHz QCPSK radio on a 15.9-mile path with and without space-diversity protection.

where T_0 = 525,600 minutes is the total annual time and r is the multipath occurrence factor,[14,27] which depends on many factors such as radio frequency, path length, path terrain, and geographic location. Figures 15 and 16 show the integrand, $[P(\text{outage}|v_{IL})p(v_{IL})]$, as a function of fade depth of the in-line signal. Most outage occurs at about 12 dB above the rms power level (i.e., 20 $\log_{10}\epsilon_{rms}$) of the residual cross-polarization interference ϵ. This is because QCPSK radio needs at least 10 dB of CIR at BER = 10^{-3} and the correlated component, kv_{IL}, of cross-polarization interference adds another 2-dB requirement. Therefore, the "effective

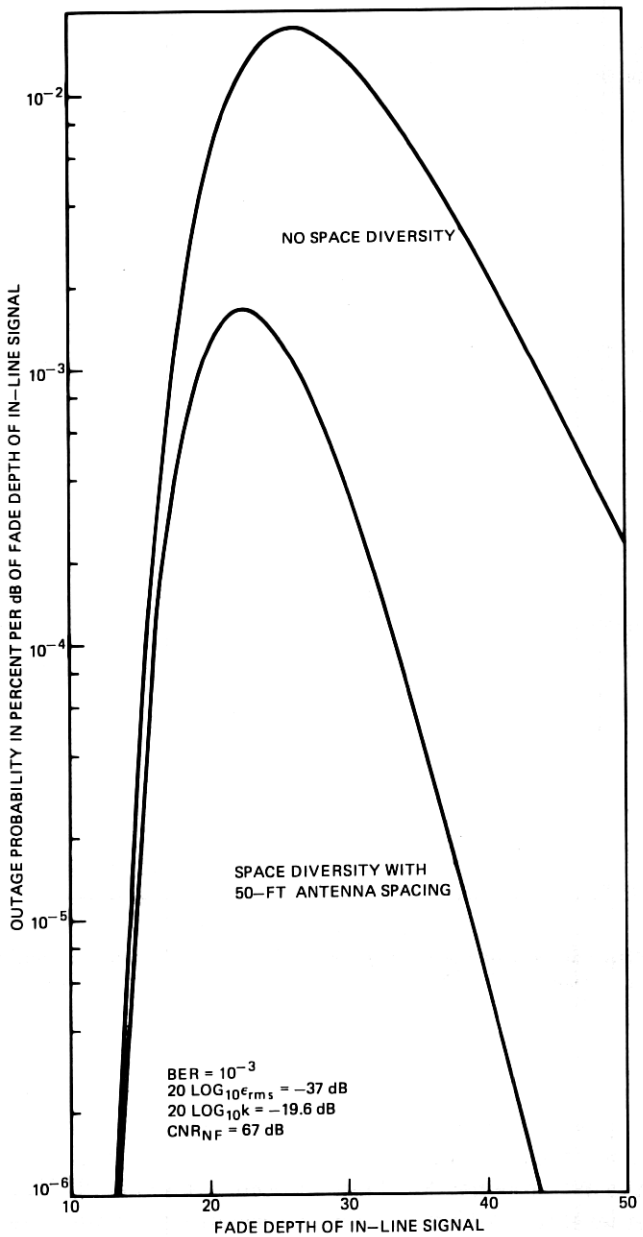

Fig. 16—Dependence of one-way outage probability density function on multipath fade depth of in-line signal of 11-GHz QCPSK radio—26.4-mile path with and without space diversity protection. Data based on multipath-caused one-way outage.

outage threshold" of dual-polarization QCPSK radio is approximately 12 dB* above ϵ_{rms}. For example, the 26.4-mile path has an effective fade margin of only 25 dB.

Notice that the thermal noise is 67 dB below the nonfaded signal level whereas this outage threshold for the 26.4-mile path is only 25 dB below the nonfaded signal level. Therefore, "multipath caused" outage of dual-polarization radio is strongly controlled by ϵ_{rms}.

(i) According to assumptions (f) and (h), the distribution of v_{IL} in the deep-fade region is

$$T(v_{IL} \leqq L) \cong rT_0L^2 \text{ for } L \leqq 0.1, \tag{33}$$

where $T(v_{IL} \leqq L)$ denotes the accumulated time per year that v_{IL} fades below L. The value of multipath occurrence factor, r, can be determined empirically by fitting eq. (33) to the measured data on $T(v_{IL} \leqq L)$. The estimated values of r for a 15.9-mile path and a 26.4-mile path near Atlanta, Georgia are given in Table I.

3.4 Results

To calculate outage probability of a radio path, we need the parameters: r, k, and ϵ_{rms} on that path. At the present time, these parameters are available only for two paths (15.9 and 26.4 miles—see Table I) measured near Atlanta, Georgia. This limits our calculations to these two particular path lengths only. The linear interpolation between these two paths lengths in Figs. 17 through 19 gives a crude estimate of outage probabilities for intermediate path lengths.

3.4.1 Effect on dual-polarization transmission

Figure 17 displays the calculated outage probabilities without diversity protection. The upper curve represents cochannel dual-polarization transmission, whereas the lower curve represents idealized single-polarization performance without cross-polarization interference and without adjacent channel interference. It is seen that the impact of a dual channelization is three orders of magnitude increase in multipath outage time. This is because the residual cross-polarization interference ϵ_{rms} is 30 dB higher than the thermal noise.

However, the idealized single-polarization performance, represented by the lower curve in Figure 17, is academic in that the impacts of adjacent channel interferences and channel dispersion during multipath fading are neglected, resulting in more than 54 dB of multipath fade margin. For a practical single-polarization-per-frequency digital system,

* 16 dB for BER = 10^{-6}.

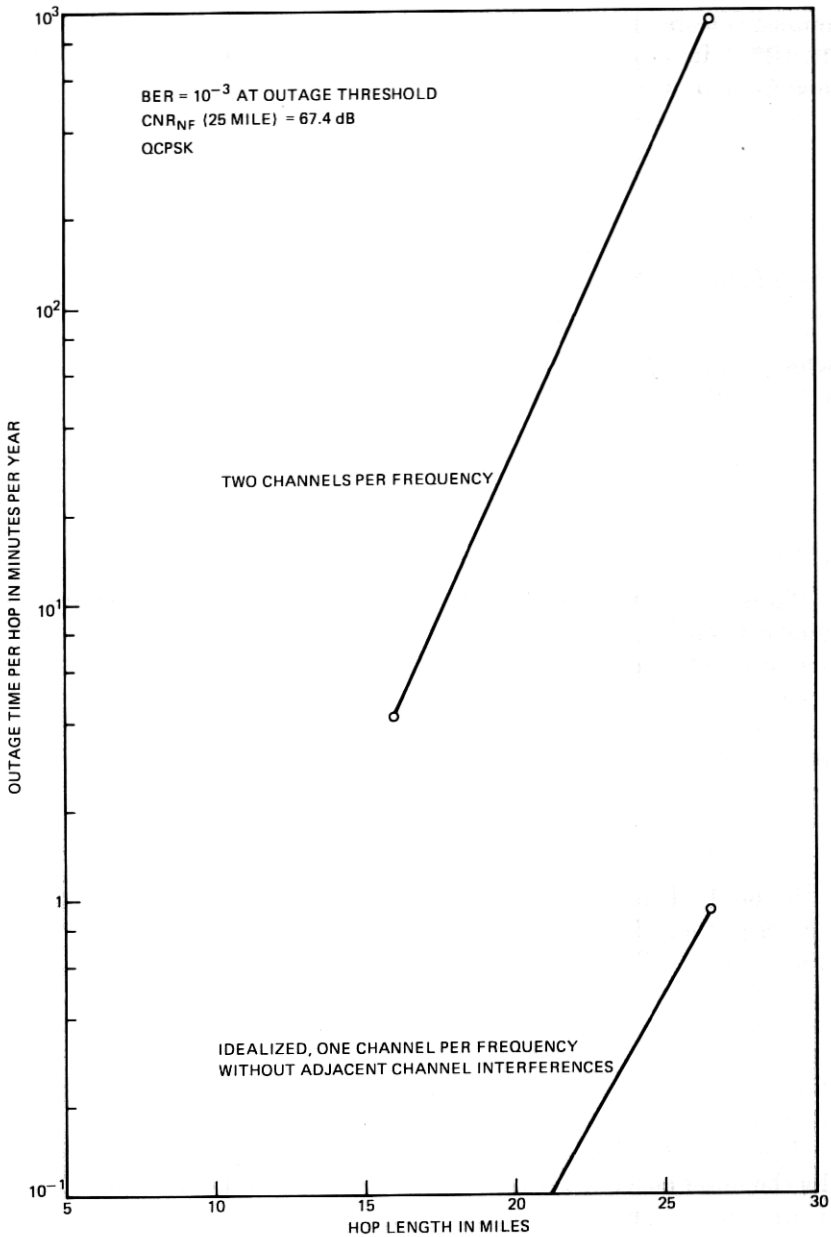

Fig. 17—The impact of cochannel dual-polarization transmission on multipath two-way outage probability of 11-GHz QCPSK radio. No space-diversity protection was provided.

the adjacent channel interferences and channel dispersion will limit the multipath fade margin to less than 35 dB and significantly increase the multipath outage time with reference to the idealized curve.

3.4.2 Space-diversity improvement

Figure 18 displays the reduction of multipath outage time through the use of space diversity. With 50-foot antenna spacing, the outage time is reduced by one order of magnitude for the 26.4-mile path and two orders of magnitude for the 15.9-mile path. The diversity improvement factor achieved by the dual-polarization digital radio is generally much smaller than we familiarly associate with a single-polarization analog radio.[24,26,27] This is because the dual-polarization digital radio has an effective fade margin of only 20 to 30 dB, whereas single-polarization analog radio generally provides a fade margin of 35 dB or more. Diversity improvement is proportional to fade margin.

3.4.3 Effect of error-rate requirement

Figure 19 shows that tightening the BER requirement at outage threshold from 10^{-3} to 10^{-6} increases the outage time by a factor of 6, even with diversity protection. This sensitivity is related to the steep inverse slope, 5 dB per decade, of fading probability of a dual-diversity signal.[12] Tightening the BER from 10^{-3} to 10^{-6} is equivalent to 4 dB (i.e., 16 to 12 dB) loss of effective fade margin.

3.4.4 Effects of ϵ_{rms} and k of interference

Figure 20 indicates that the outage probability is extremely sensitive to the power level, ϵ_{rms}, of the residual cross-polarization interference. A 10-dB decrease in ϵ_{rms} will reduce outage probability by two orders of magnitude. Again, this is related to the steep, inverse slope of 5 dB per decade of fading probability for a dual-diversity signal.

On the other hand, Figure 21 shows that the outage probability is practically independent of the correlated components (kv_{IL}) of cross-polarization interference as long as $20 \log_{10} k \leqq -30$ dB. This is intuitively obvious because this component of CIR is constant. As long as CIR $\geqq 30$ dB, the interference has negligible effect on QCPSK radio (see CNR versus CIR curve in Fig. 14). In practice, this means it is of questionable benefit to improve XPD of a radio link beyond 30 dB, during periods of normal propagation. The controlling factor on outage time is the residual cross-polarization, ϵ, which is typically 10 dB or more below kv_{IL} and is almost unobservable during a nonfading period. Therefore, the under-

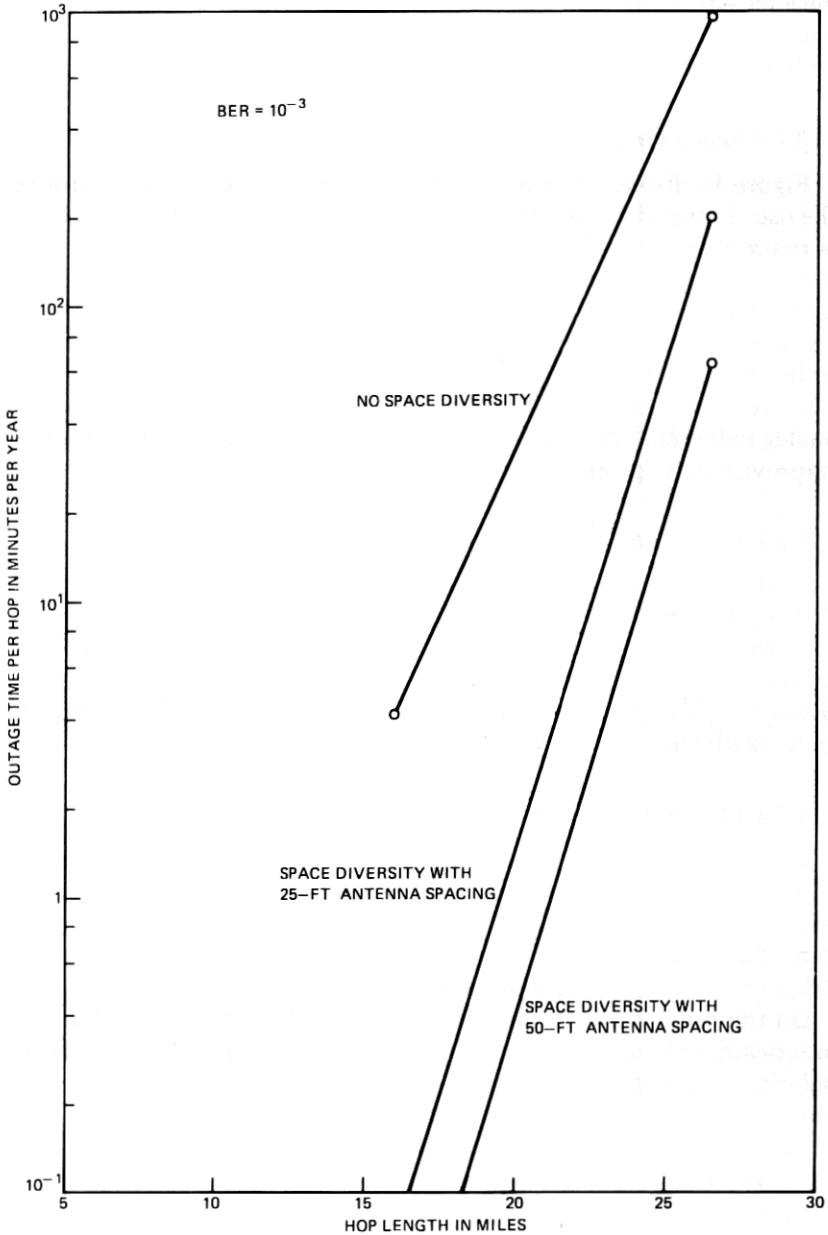

Fig. 18—Effect of space-diversity protection on multipath two-way outage probability of 11-GHz dual-polarization QCPSK radio.

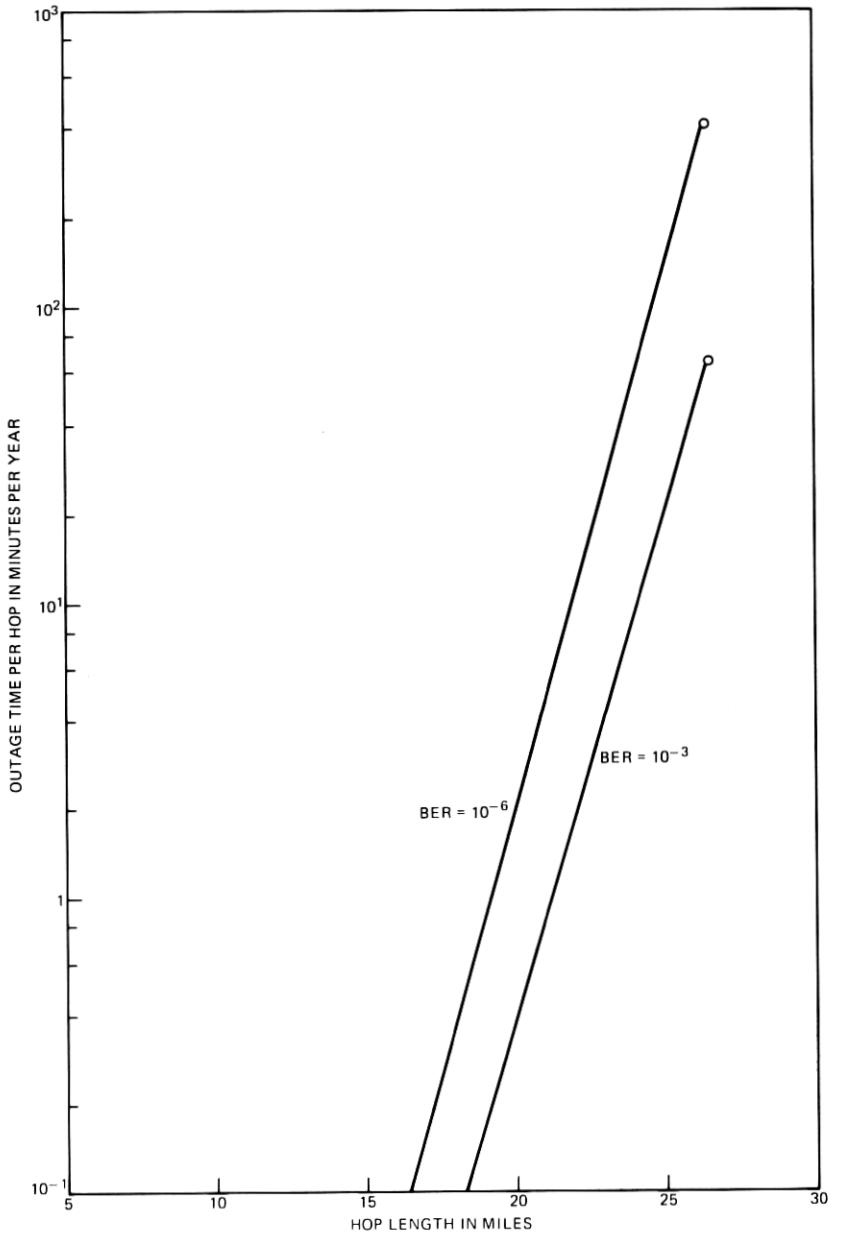

Fig. 19—Effect of bit-error-rate requirement at outage threshold on multipath two-way outage probability of 11-GHz dual-polarization QCPSK radio—with space diversity and 50-foot antenna spacing.

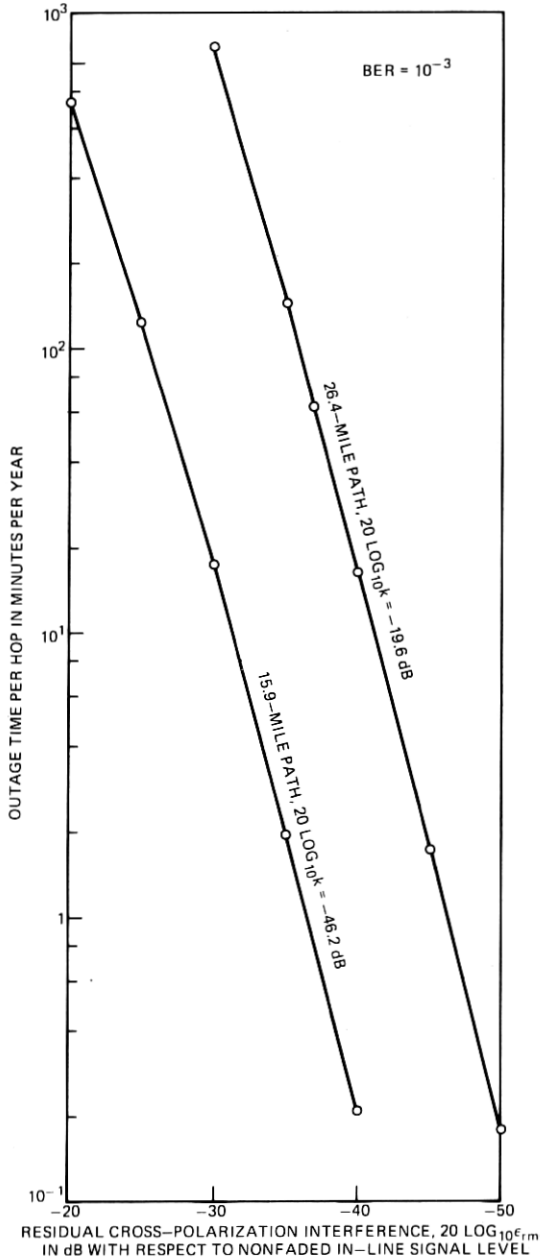

Fig. 20—Sensitivity of multipath two-way outage probability of 11-GHz dual-polarization QCPSK radio on the rms value, ϵ_{rms}, of the residual component of cross-polarization interference—with space diversity and 50-foot antenna spacing.

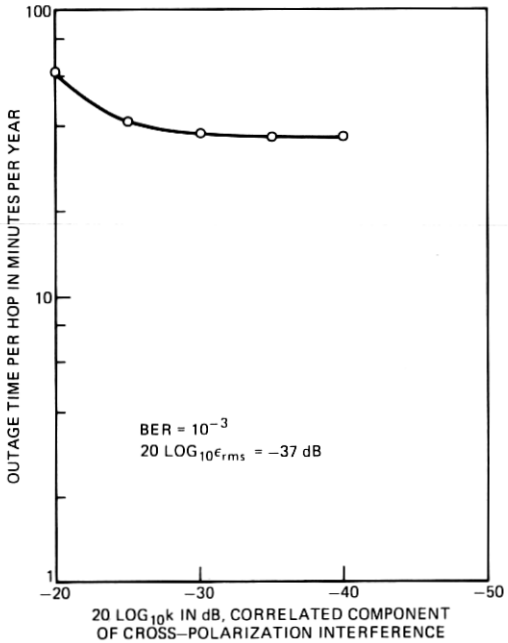

Fig. 21—Dependence of multipath two-way outage probability of 11-GHz dual-polarization QCPSK radio on the correlated component, kv_{IL}, of cross-polarization interference—with space diversity, 50-foot antenna spacing, and 26.4-mile path.

standing and identification of major contributors of the residual cross-polarization interference ϵ are important subjects for future study.

3.4.5 Effect of thermal noise

The effects of varying CNR_{NF} on outage probability are shown in Fig. 22. Since CNR_a = 13.4 dB, at BER = 10^{-3}, assumption (a) implies a 54-dB fade margin* in the absence of the interference.[22] Figure 22 shows it is also not of benefit to suppress the thermal noise level below the level, $\epsilon_{rms} - \Delta$, of residual cross-polarization interference as far as multipath outage† is concerned. As long as the noise level is below $\epsilon_{rms} - \Delta$, the multipath outage is controlled by ϵ_{rms} and is independent of noise level.

3.5 Some qualifications

3.5.1 Effect of channel dispersion during multipath fading

A quaternary PSK signal is equivalent to two streams of binary PCM signals, each phase modulating a carrier of the same frequency, but with

* The fade margin is reduced to 48 dB during rain because of 4-dB wet radome attenuation and 2-dB degradation by rain-induced depolarization.

† On the other hand, reducing the noise level will reduce rain-caused outage time.

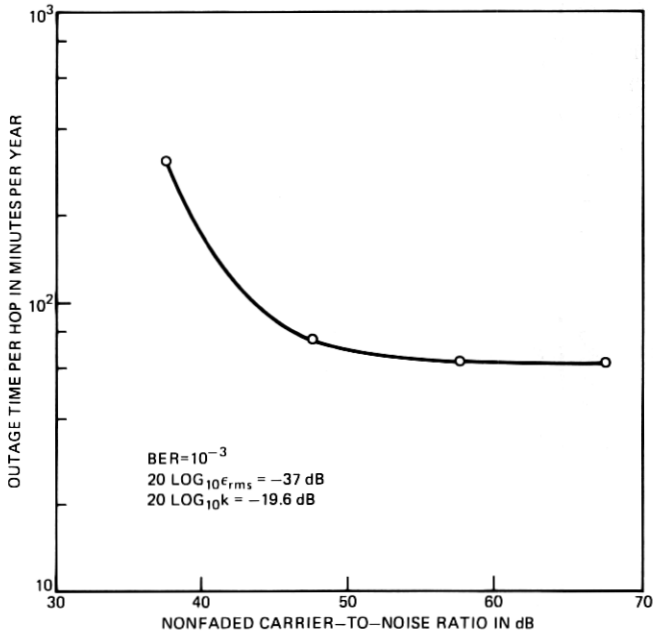

Fig. 22—Effect of reducing thermal noise level on the multipath two-way outage probability of 11-GHz dual-polarization QCPSK radio—with space diversity, 50-foot antenna spacing, and 26-mile path length.

90-degree phase shift.[22] Therefore, cochannel dual-polarization QCPSK radio requires the following two orthogonalities for successful transmission:

(*i*) Polarization orthogonality between the cochannel pair.
(*ii*) Phase orthogonality between the two streams of binary PSK signals.

Multipath fading, with channel dispersion, will degrade both polarization and phase orthogonalities. At the present time, our understanding of degradation of phase orthogonality during multipath fading is insufficient for outage calculations. Therefore, the possible outages due to crosstalk between the two orthogonally phased carriers are unaccounted for in this paper.

3.5.2 Limitation of available path parameters

All the calculations in this report are based on measured path parameters: r, k, and ϵ_{rms}, pertinent to two paths near Atlanta, Georgia. The variations of k and ϵ_{rms} parameters with time base, path length, and geographic location are not understood.

3.5.3 Relationship between CNR and CIR

The CNR versus CIR relationship for QCPSK radio (Fig. 14) is based on presently available hardware technology. This behavior is several dB poorer than the idealized relationship in Refs. 28 and 29. Future advances may improve this behavior and reduce the outage time.

IV. CONCLUSION

A microwave propagation experiment near Atlanta, Georgia has provided statistics describing depolarization during multipath fading at 6 and 11 GHz on two paths (15.9 and 26.4 miles). Data gathered over a 6.5-month period have been processed and presented. These data are supportive of a model in which the depolarized signal (interference) consists of a component correlated with the in-line signal, and a residual component independent of the in-line signal. The residual component is Rayleigh distributed with a typical rms value about 40 dB below the nonfaded in-line signal. The cross-polarization interference, conditioned to a given in-line signal level, is Rice-Nakagami distributed. The calculated Rice-Nakagami distribution fit these 6.5-month data very closely.

The experimental data and theoretical model are applied to estimate the multipath outage probability of cochannel dual-polarization 11-GHz QCPSK digital radio affected by thermal noise and cross-polarization interference during multipath fading. Detailed results are given in Section 3.4.

V. ACKNOWLEDGMENTS

I wish to express appreciation to T. O. Mottl for valuable discussion on this topic and to M. V. Pursley, P. L. Dirner, and R. K. Graef for assistance in data processing. The radio equipments in this propagation experiment were assembled and installed by L. J. Morris.

REFERENCES

1. W. T. Barnett, "Degradation of Cross-Polarization Discrimination During Rain and Multipath Fading at 4 GHz," IEEE 1974 International Conference on Communications, June 17–19, 1974, Minneapolis, Minnesota, Conference Record, pp. 12D-1—12D-4, IEEE Cat. No. 74, CHO 859-9-CSCB.
2. K. Morita, "Fluctuation of Cross-Polarization Discrimination Ratio Due to Fading," Rev. of Elec. Commun. Lab., *19*, No. 5–6 (May-June 1971), pp. 649–652.
3. T. Inoue and T. Akiyama, "Propagation Characteristics of Line-of-Sight Oversea Paths in Japan, "IEEE Trans. Ant. Propag., *AP-22*, No. 4 (July 1974), pp. 557–565.
4. T. Inoue, "Microwave Oversea Circuit Cross-Polarization Distortion Characteristics," Rev. Elec. Commun. Lab., *23*, No. 3–4 (March-April 1975), pp. 374–386.
5. G. Lefrancois, L. Martin, and M. Rooryck, "Influence of the Propagation on the Value

of the Decoupling of Two Orthogonal Polarizations," Ann. Telecommun., *28* (1973), pp. 316–324.
6. T. O. Mottl, "Dual-Polarized Channel Outages During Multipath Fading," B.S.T.J., this issue, pp. 675–701.
7. R. W. Friis and A. S. May, "A New Broadband Microwave Antenna System," Commun. Electron., No. 35 (March 1958), pp. 97–100.
8. E. T. Harkless, "A Network for Combining Radio Systems at 4, 6 and 11 kmc," B.S.T.J., *36* (September 1957), pp. 1253–1267.
9. M. A. Gerdine and H. F. Lenzing, "Reduction of Delay Distortion in a Horn-Reflector Antenna System Employing Overmoded-Waveguide Feeder," IEEE Trans. Commun. Technol., *COM-18,* No. 1 (February 1970), pp. 21–26.
10. P. I. Sandsmark, "Effect of Ellipticity on Dominant-Mode Axial Ratio in Nominally Circular Waveguides," IRE Trans. Microw. Theory Tech., *MTT-3,* No. 5 (October) Vol. 1955, pp. 15–20.
11. S. H. Lin, "Statistical Behavior of a Fading Signal," B.S.T.J., *50,* No. 10 (December 1971), pp. 3211–3270.
12. S. H. Lin, "Statistical Behavior of Deep Fades of Diversity Signals," IEEE Trans. Commun., *COM-20,* No. 6 (December 1972), pp. 1100–1107.
13. A. Vigants, "Number and Duration of Fades at 6 and 4 GHz," B.S.T.J., *50* (March 1971), pp. 815–841.
14. W. T. Barnett, "Multipath Propagation at 4, 6 and 11 GHz," B.S.T.J., *51,* No. 2 (February 1972), pp. 321–361.
15. S. O. Rice, "Mathematical Analyses of Noise," B.S.T.J., *23* (July 1944), pp. 282–332, and *24* (January 1945), pp. 46–256.
16. M. Nakagami, "The m-Distribution—A General Formula of Intensity Distribution of Rapid Fading," in W. C. Hoffman (ed.), *Statistical Methods in Radio Wave Propagation,* Oxford: Pergamon, 1960.
17. P. Beckmann, *Probability in Communication Engineering,* New York: Harcourt, Brace & World, 1967.
18. E. T. Harkless and H. F. Lenzing, "Excitation of Higher Order Antenna Modes by Multipath Propagation," IEEE Trans. Commun. Technol., *COM-15,* No. 4 (August 1967), pp. 567–603.
19. H. F. Lenzing, "Higher Order Mode Excitation in Larger Aperture Receiving Antennas," Microw. J., *12,* No. 12 (December 1969), pp. 61–65.
20. S. H. Lin, "A Method for Calculating Rain Attenuation Distributions on Microwave Paths," B.S.T.J., *54,* No. 6 (July-August 1975), pp. 1051–1086.
21. Unpublished work.
22. A. J. Giger and T. L. Osborne, "3A-RDS 11 GHz Digital Radio System," 1976 International Conference on Communications, Philadelphia, Pennsylvania, June 14–16, Conference Record, pp. 18-1—18-7, *IEEE Cat.,* No. 76CH1085-0, CSCB, Vol. II.
23. H. Staras, "Diversity Reception with Correlated Signals," J. Appl. Phys., *27,* No. 1 (January 1956), pp. 93–94.
24. A. Vigants, "Space Diversity Performance for Antennas of Unequal Size and Correlated Rayleigh Fading," unpublished work.
25. R. H. Clarke, "A Statistical Theory of Mobile-Radio Reception," B.S.T.J., *48* (August 1969), pp. 957–1000.
26. A. Vigants, "Space Diversity Performance as a Function of Antenna Separation," IEEE Trans. Commun. Technol., *COM-16,* No. 5 (December 1969), pp. 831–836.
27. A. Vigants, "Space Diversity Engineering," B.S.T.J., *54,* No. 1 (January 1975), pp. 103–142.
28. A. S. Rosenbaum, "PSK Error Performance with Gaussian Noise and Interference," B.S.T.J., *48,* No. 2 (February 1969), pp. 413–442.
29. V. K. Prabhu, "Error Rate Considerations for Coherent Phase-Shift Keyed Systems with Cochannel Interference," B.S.T.J., *48,* No. 3 (March 1969), pp. 743–767.